NINTH EUROPEAN ROTORCRAFT FORUM

Paper No. 52

ROTORCRAFT AIR RESONANCE IN FORWARD FLIGHT WITH VARIOUS DYNAMIC INFLOW MODELS AND AEROELASTIC COUPLINGS

J. NAGABHUSHANAM

Hindustan Aeronautics Limited,
(Bangalore)
INDIA

and

G.H. GAONKAR

Indian Institute of Science
(Bangalore)
INDIA

September 13-15, 1983

STRESA, ITALY

Associazions Industrie Aerospaziali

Associazione Italiana di Aeronautica ed Astronautica

ROTORCRAFT AIR RESONANCE IN FORWARD FLIGHT WITH VARIOUS DYNAMIC INFLOW MODELS AND AEROELASTIC COUPLINGS

J. Nagabhushanam
Hindustan Aeronautics Limited,
Bangalore, India

G.H. Gaonkar
Indian Institute of Science,
Bangalore, India

SUMMARY

Air Resonance with Dynamic Inflow is studied in forward flight ($0 \leq$ advance ratio ≤ 0.4). Effects of trimming conditions and parameters such as lag structural damping, blade and body inertias and aeroelastic couplings are included. Two models from an unsteady actuator-disk theory are used, a 5x5 model and its 3x3 analogue according to second and first harmonic inflow distributions respectively. The 3x3 model reduces to the momentum theory model under axial flow conditions. For the 5x5 inflow model, the damping data of (rotor/body) systems are physically inconsistent for rotors with 3 and 4 blades, whereas they are consistent for rotors with 5 and more blades. The nature of this inconsistency concerning multiblade and body modes is further explored, complementing the findings of an earlier study. A five bladed system with the 5x5 inflow model is taken as a baseline configuration for correlation purposes. The 3x3 model gives consistent damping data for systems with 3 and more blades and excellent correlation. It is used in the parametric analyses over a broad spectrum of inplane and flapping frequencies, and systems with favourable air resonance characteristics are identified. The basic characteristics of air resonance are not sensitive to the number of blades perse, though they are, to trimming conditions. The stability margin of the lag regressing mode in the hovering could worsen in forward flight, particularly for the soft inplane rotors in propulsive trim and for the stiff inplane rotors in moment or wind-tunnel trim.

NOTATION

a	Lift curve slope
c	Blade chord
C_L	Harmonic perturbation of roll moment coefficient
C_M	Harmonic perturbation of pitch moment coefficient
C_{2L}, C_{2M}	Second harmonic pressure perturbation coefficients for roll and pitch
C_T	Harmonic perturbations of thrust coefficient (also steady thrust coefficient in figures)

c_d	Profile drag coefficient
$\bar{f}$	Dimensionless helicopter flat plate area
$\bar{F}_\beta$	Dimensionless force per unit length perpendicular to the blade and direction of rotation
$\{F\}$	Harmonics of disc loading
$\bar{h}$	Distance from rotor centre to body centre of mass (h)/ rotor radius (R)
K_β, K_ζ	Spring stiffnesses at the rotor centre in flap and lag
$[L]$ & $[M]$	Dynamic inflow and apparent mass matrices
m	Mass of the blade
m_f	Mass of the rotor-support system or body
m_μ	Mass ratio, $Nm/(Nm + m_f)$
N	Number of blades
P	Dimensionless rotating uncoupled flap frequency
R	Radius of the blade and also hub rigidity or elastic coupling parameter
$\bar{r}_c$ ($\bar{r}_s$)	Body mass radius of gyration in pitch (roll)/ rotor radius
t	Dimensionless time (identical with the blade azimuth position of the first blade ψ_1)
$\{V\}$	Inflow vector
v	Flow rate parameter
x	Blade radial coordinate/rotor radius
$\bar{\alpha}_c(\alpha_c)$	Steady (Perturbed) state body roll
$\bar{\alpha}_s(\alpha_s)$	Steady (Perturbed) state body pitch
α_{sh}	Rotor shaft angle or incidence angle
$\beta_k(\zeta_k)$	Perturbed flap (lag) angle of the k-th blade
$\beta_o(\zeta_o)$, $\beta_s(\zeta_s)$, $\beta_c(\zeta_c)$, $\beta_{2s}(\zeta_{2s})$ & $\beta_{2c}(\zeta_{2c})$	Multiblade flapping (lag) coordinates: Collective, first order cyclic and second order cyclic flapping (lag) components
$\beta_d(\zeta_d)$	Multiblade flap (lag) differential collective coordinate
$\bar{\beta}_k(\bar{\zeta}_k)$	Equilibrium flapping angle (lag) of the k-th blade: $=\bar{\beta}_o(\bar{\zeta}_o) + \bar{\beta}_s(\bar{\zeta}_s)\ \mathrm{Sin}\psi_k + \bar{\beta}_c(\bar{\zeta}_c)\ \mathrm{Cos}\psi_k$

β_{pc}	Precone
γ	Lock number ($3\ \rho acR^2/m$)
ε	A small parameter of the ordering scheme
η_ζ	Lag structural damping ratio
θ_k	See equation (6)
θ_β, θ_ζ	Pitch-flap and pitch-lag coupling ratios
λ	Total induced flow
$\overline{\lambda}$	Steady inflow (free stream plus induced flow)
$\overline{\nu}$	Steady induced flow
ν	Inflow perturbation
ν_o, ν_s, ν_c, ν_{2s} & ν_{2c}	Inflow perturbation components, see equation (3)
ρ	Air density
σ	Solidity ratio ($Nc/\pi R$)
ψ	Spatial azimuth position
ψ_k	Azimuth angle of the k-th blade (identical to t) $\psi_K = (2\pi/N)(k-1)+t$
ω_ζ	Dimensionless uncoupled lag frequency
μ	Advance ratio
Ω	Rotor speed
$(.)$	$\frac{d}{dt}$ ( )

1. Introduction

Air resonance remains a stability problem of air-borne helicopters with hingeless and bearingless rotors[1-2]. As a low frequency phenomenon, it is essentially the frequency coalescence of the lag regressing mode and the body (rotor support) mode, normally the body pitch or roll mode. It is also an asymmetrical phenomenon, where the roll mode is usually more critical owing to its low inertia. While air resonance perse is induced by the relatively high stiffness of the flap regressing mode, its severity is due to the inherently small lag damping, typical of non-articulated rotors[1-2]. Finding judicious combinations of aeroelastic couplings that can provide adequate damping levels for the entire flight regime is not only challenging but also an urgent problem[2]. Though hingeless rotors have been equipped with auxiliary lag dampers, such a measure is cost ineffective and at best remedial.

Under axial flow conditions (e.g. hovering), air resonance has been well researched with the help of conceptual models and many aspects of it have been explained[1-8]. For example, increasing blade pitch is generally destabilising and appropriate combinations of aeroelastic couplings have beneficial effects[1,3-7]. On the effect of dynamic inflow, two recent findings should be mentioned[4]. First, dynamic inflow increases lag regressing mode damping and significantly decreases body roll mode damping. Second, the widely held premise that dynamic inflow would be destabilising at low thrust and essentially negligible at high thrust is of limited validity[4]. These findings have been further corroborated with test data[3,5,6,8].

By comparison, in forward flight, only a small beginning has been made which indicates in general, the stabilising influence of forward flight on air resonance[8-10]. Reference 8 to 10 give a good account of air resonance. However, they are basically oriented towards specific configurations persued by the respective industries. As such, they are not oriented towards a broad spectrum of rotor/body configurations with emphasis neither on the physics of air resonance, nor towards mapping out configurations with favourable air resonance characteristics. Given the sensitivity of low-frequency instabilities to trimming conditions[11] and dynamic inflow[4], an improved understanding of air resonance would require such a treatment with dynamic inflow for different trimming conditions. Recently, King[8] has provided the validation for the predicted air resonance data with the benefit of test data for hovering conditions, with incidental reference to forward flight conditions. In Reference 9, a complex global model is described to predict designworthy damping data which correlate with wind tunnel model and flight test data. Reference 10 studies the problem of a flight control system on air resonance, as a means of minimising the influence of flapping dynamics in the coupled rotor/body dynamics. Successful utilisation of flight control system feedback would depend upon how well the problem of air resonance is understood, particularly in forward flight. This problem is still in the developmental stages[10,12].

An exploratory study is pursued here in several phases concerning: 1) selection of a viable dynamic inflow model[13-16]; 2) sensitivity to trimming procedures, and to number of blades and 3) judicious use of system parameters and aeroelastic couplings to improve air resonance characteristics. Concerning these phases, it is advanced over the preceding

studies[8-11,13-16] in several respects:

1. It considers the rotor/body systems with 3, 4 and 5 blades in combination with two dynamic inflow models from an unsteady actuator disk theory[15,16] - - a 3x3 model which reduces to the momentum theory model in hover and its 5x5 analogue. In reference 16, hub-fixed flap-lag stability of rotors with 3 and 5 blades in forward flight is treated with a hierarchy of inflow models to assess the consistency of these models. Here, this aspect is comphrehensively explored for rotor/body systems with respect to multiblade and body modes. New information is provided particularly for body modes for N = 3, 4 and 5 and for lag collective and differential collective modes for N = 4.

2. It includes the corresponding quasi-steady models, since inflow is virtually quasi-steady for large advance ratios ($\mu \geq 0.25$) and since quasi-steady inflow effects can be accounted for with relatively less computations[13,14,16].

3. It treats air resonance for advance ratios varying from 0 to 0.4, under propulsive (flight) and moment (wind-tunnel) trim conditions, typical of main rotors, and also under untrim (unrestricted tip-path plane) conditions, typical of tail rotors. Accordingly, both soft and stiff inplane rotors are included.

4. It considers whether the number of blades perse is an important parameter in assessing the principal effects of air resonance.

5. It treats the effects of (rotor/body) system parameters such as aeroelastic couplings, structural damping etc., to assess how far these parameters that stabilise air resonance in hover[1-8], affect air resonance in forward flight.

2. Inflow and Rotor/Body Systems (N ≥ 3)

We will consider, from an unsteady actuator disk theory two dynamic inflow models - - a 3x3 model and its 5x5 analogue. This 3x3 model reduces to the momentum theory model under axial flow conditions[16]. The dynamic inflow ν is perturbed with respect to the steady inflow $\bar{\lambda}$, and the total induced flow λ, is given by

$$\lambda = \bar{\lambda} + \nu \tag{1}$$

In forward flight when the steady inflow is non-uniform, the average inflow angle $\bar{\phi}$ can be reasonably approximated by the integral[14].

$$\bar{\phi} = 4 \int_0^1 \bar{\lambda}\, r^2\, dr \tag{2}$$

We now represent ν at a point (x,ψ) in the rotor disk as[16]

$$\nu = \nu_0 + \nu_s x \sin\psi + \nu_c x \cos\psi + \nu_{2s} x^2 \sin 2\psi + \nu_{2c} x^2 \cos 2\psi \tag{3}$$

The components of inflow (ν_o, ν_s, ν_c, ν_{2s}, ν_{2c}) and the transient disk air loads (C_T, C_L, C_M, C_{2L}, C_{2M}) are governed by the first-order

perturbed linear model[16], viz

$$[m_{ij}] \begin{Bmatrix} \nu_0 \\ \nu_s \\ \nu_c \\ \nu_{2s} \\ \nu_{2c} \end{Bmatrix} + [L_{ij}]^{-1} \begin{Bmatrix} \nu \\ \nu_s \\ \nu_c \\ \nu_{2s} \\ \nu_{2c} \end{Bmatrix} = \begin{Bmatrix} C_T \\ C_L \\ C_M \\ C_{2L} \\ C_{2M} \end{Bmatrix}, \quad i,j=1,\ 2,\ ..\ 5 \qquad (4a)$$

which is expressed symbolically as

$$[\,m\,]\ \{\dot{V}\} \ + \ [\,L\,]^{-1}\ \{V\} \ = \ \{F\} \qquad (4b)$$

where the 5x5 apparent mass matrix $[\,m\,]$ and the 5x5 inflow matrix $[\,L\,]$ are shown in tables 1 and 2. For rotors with a finite number of blades, the right hand side of equation (4b) or $\{F\}$, has to be approximated by the following instantaneous functions of the blade loading:

$$C_T = + \frac{a\sigma}{\gamma N} \sum_{k=1}^{N} \left(\int_0^1 (\bar{F}_\beta)_k \, dx \right) \qquad (5a)$$

$$C_L = - \frac{a\sigma}{\gamma N} \sum_{k=1}^{N} \left(\int_0^1 (\bar{F}_\beta)\, x \, dx \right) \sin\psi_k \qquad (5b)$$

$$C_M = - \frac{a\sigma}{\gamma N} \sum_{k=1}^{N} \left(\int_0^1 (\bar{F}_\beta)_k \, x \, dx \right) \cos\psi_k \qquad (5c)$$

$$C_{2L} = - \frac{a\sigma}{\gamma N} \sum_{k=1}^{N} \left(\int_0^1 (\bar{F}_\beta)_k \, x^2 \, dx \right) \sin 2\psi_k \qquad (5d)$$

$$C_{2M} = - \frac{a\sigma}{\gamma N} \sum_{k=1}^{N} \left(\int_0^1 (\bar{F}_\beta)_k \, x^2 \, dx \right) \cos 2\psi_k \qquad (5e)$$

The 3x3 model does not have the second harmonic components ν_{2s} and ν_{2c}. Therefore, the corresponding elements of the 3x3 matrices $[\,m\,]$ and $[\,L\,]$ and the 3x1 disk loading vector $\{F\}$ are obtained by the elimination of the terms pertaining to ν_{2s} and ν_{2c} in tables 1 and 2.

As to the rotor/body system, the analytical model is identical to the one developed in reference 1, it is used in reference 4 and is quite similar to the one of reference 8 as well. Figure 1 shows its schematic together with the block diagram of inflow dynamics. Small (x,y,z) refers to the rotating coordinate system, rotating with angular velocity Ω, whereas, capital (X,Y,Z), refers to the non-rotating coordinate system. The straight and slender rigid blades have only flap and lag degrees of freedom. They are flexibly attached at the rotor centre with flap and lag restraint springs which are perpendicular and parallel to the blade chord line respectively. These spring stiffnesses, k_β and k_ζ, are selected such that the uncoupled rotating flap and lag natural frequencies coincide with the corresponding first-mode rotating natural frequencies of the elastic blade. Quasi-steady

Table - 1

Elements of M-matrix (diagonal)

m_{11}	m_{22}	m_{33}	m_{44}	m_{55}
$\frac{8}{3\pi}$	$-\frac{16}{45\pi}$	$-\frac{16}{45\pi}$	$-\frac{256}{1575\pi}$	$-\frac{256}{1575\pi}$

Table - 2

Elements of L-matrix

$$L = 1/v \begin{bmatrix} \frac{1}{2} & 0 & \frac{15\pi}{64}\sqrt{\frac{(1-\sin\alpha)}{(1+\sin\alpha)}} & 0 & 0 \\ 0 & \frac{-4}{(1+\sin\alpha)} & 0 & \frac{105\pi\ (1-\sin\alpha)}{128\ \ (1+\sin\alpha)} & 0 \\ \frac{15\pi}{64}\sqrt{\frac{(1-\sin\alpha)}{(1+\sin\alpha)}} & 0 & \frac{-4\ \sin\alpha}{1+\sin\alpha} & 0 & \frac{3\pi\ \sin\alpha(1-\sin\alpha)}{4} \\ 0 & \frac{-45\pi\ (1-\sin\alpha)}{32\ \ (1+\sin\alpha)} & 0 & \frac{-\sin\alpha(11-5\ \sin\alpha)}{(1+\sin\alpha)} & 0 \\ \frac{-3\ (1-\sin\alpha)}{7\ (1+\sin\alpha)} & 0 & -2\ \sin\alpha(1-\sin\alpha) & 0 & \frac{-6\ (1+\sin^2\alpha)}{(1+\sin\alpha)^2} \end{bmatrix}$$

where $v = (\mu^2 + \bar{\lambda}\ (\bar{\lambda} + \bar{\nu}))\ /\ \sqrt{\mu^2 + \bar{\lambda}^2}$

linear airfoil aerodynamics is used without the inclusion of nonlinear effects such as stall and compressibility. The dimensionless time t, (with time unit $1/\Omega$), is equal to the azimuth angle of the reference blade ψ_1. The hub-flexibility (inboard of the blade location where pitch change takes place) is simulated by introducing an elastic coupling parameter R which relates the rotation of the principal axes of the blade-hub system and the blade pitch θ. Blade torsional flexibility is included in a quasi-steady manner by expressing θ of the k-th blade as

$$\theta_k = \theta_o + \theta_s \sin\psi_k + \theta_c \cos\psi_k + \theta_\beta \beta_k + \theta_\zeta \zeta_k + \theta_\beta(\beta_k - \beta_{pc}) \qquad (6)$$

where θ_β is pitch-flap coupling and θ_ζ pitch-lag coupling.

The rotor-support system is idealized as a rigid body with roll and pitch degrees of freedom. Given the low-frequency characteristics of air resonance, this model should prove adequate to estimate the principal effects of air resonance qualitatively. The formulation of the state equations for the rotor-body systems with feedback from the unsteady and quasi-steady inflow follows on similar lines of several earlier studies on flap-lag stability with dynamic inflow[4,11,14,16]. For specific details which includes body motions see reference 17.

3. Numerical Results

Air resonance data refer to three equilibrium positions - - wind tunnel trim (moment trim, $\bar{f} = 0$), propulsive trim (moment trim, $\bar{f} = 0.01$) and untrim ($\bar{f} = 0$). It is assumed that steady lag, body roll and pitch motions are zero ($\bar{\zeta}_k = \bar{\alpha}_s = \bar{\alpha}_c = 0$). For both the moment trim conditions, typical of main rotors, the cyclic pitch components θ_s and θ_c are adjusted so as to have zero roll and pitch moments at the hub ($\bar{\beta}_s = \bar{\beta}_c = 0$). For the untrimmed case, $\theta = \theta_o$ and $\theta_s = \theta_c = 0$, (with an unrestricted tilt of the tip-path plane) i.e. $\bar{\beta}_s \neq 0$ and $\bar{\beta}_c \neq 0$, typical of tail rotors. The parasite drag is neglected in the wind tunnel trim and untrim. However, we account for it in the propulsive trim by tilting the shaft and using the concept of an equivalent flat plate area $\bar{f}$. For pure helicopters, shaft tilt usually varies from 5 to 9 degrees in cruising. Thus, for small shaft tilt or incidence angle α_{sh}, we have $\bar{\lambda} = \alpha_{sh}\mu + \bar{\nu}$, for $\bar{f} \neq 0$, and $\bar{\lambda} = \bar{\nu}$ for $\bar{f} = 0$. Details of trim formulation including the case of non-zero hinge offset ($e \neq 0$), are in reference 17. While deriving the state equations for the rotor-body-inflow system, we have introduced a small parameter ε of the order of $\bar{\lambda}$, $\bar{\beta}_k$, $\bar{\theta}_k$, $\sqrt{c_d/a}$ etc. The state equations are generated for the ordering scheme $1 >> \varepsilon^2$, by a symbolic processor[18]. In the hovering, the generated equations have been found to agree term-by-term with manually derived ones[4] for the ordering scheme. In forward flight spot-checks of the generated equations have also revealed agreement with the manually derived expressions such as the coefficients of $\dot{\zeta}_s$ etc.

The dynamic inflow matrix L in table 2 is evaluated for a given value of advance ratio μ by identifying the shaft-tilt or incedence angle α_{sh} with the wake skew angle down stream of the rotor such that $\alpha_{sh} = \tan^{-1}(\lambda/\mu)$.

Computational details of Floquet eigenvalues are as in reference 13. The difficulty of identifying modes from a Floquet analysis is substantially overcome with concomitant analyses of the corresponding constant parameter system and of modal vectors of the corresponding Floquet transition

matrix. It should be noted that in forward flight, particularly for $\mu > 0.2$ or so, the terms lag regressing mode, roll mode etc., have diminished physical significance since the modes are coupled significantly. In the presentation of data, lag regressing, body roll and body pitch modes are emphasized, since air resonance is intrincically governed by these modes. The numerical results refer not only to the parameter values of the base-line configuration, but also to additional values as shown in table 3. When a particular parameter value differs from the corresponding base-line value, it is appropriately identified.

Numerical results are presented in four phases concerning; 1) selection of a consistent dynamic inflow model ($N \geq 3$) and quasi-steady approximation; 2) sensitivity to the number of blades and trim; 3) effects of the structural lag damping, body inertia, Lock number and mass ratio and 4) effects of aeroelastic couplings for varying flap and lag frequencies. More details and data including hinge offset effects, are in reference 17.

TABLE 3

Rotor/Body/Inflow System Parameters for Numerical Results

Parameters	Base-line values	Additional values
μ	0.3	Variable (0 - 0.4)
γ	5.0	Variable (3 - 10)
Elastic Coupling R	0.0	Variable (0 - 1)
P	1.15	Variable (1 - 1.35)
ω_ζ	0.7	Variable (0.1 to 1.9)
C_T/σ	0.2	Variable (0.05 to 0.35)
σ	0.05	---
N	5.0	Variable (3, 4)
c_d/a	$0.01/2\pi$	---
m_μ	0.1	Variable (0.06 to 0.16)
$\bar{r}_c$	0.4	Variable (0.3 to 0.48)
$\bar{r}_s$	0.2	Variable (0.125 - 0.275)
$\bar{h}$	0.4	---
θ_β	0.0	Variable (-0.4 to 0.4)
θ_ζ	0.0	Variable (-0.3 to 0.3)
α_{sh}	$\tan^{-1}(\bar{\lambda}/\mu)$	---
Equilibrium conditions	Moment trim ($\bar{f} = 0.0$)	Propulsive trim ($\bar{f}$=0.01) and untrim ($\bar{f} = 0.0$)
η_ζ	0.0	0 - 0.015

For the numerical results to follow it is appropriate to mention that they are based on several over simplified assumptions[17] with respect to trimming, modeling the rotor/body system etc. Though quantitatively these results may require corrections, the established trends should provide useful approximation to an accurate measure of air resonance boundaries and stability margins.

We begin with phase I which was discussed in reference 16 for a hub-fixed rotor system with 3 and 5 blades. The data that are presented here give new information on the body modes for N = 3, 4 and 5 and also on the lag differential collective mode (N = 4). The results of figure 2, show the damping levels of the lag regressing mode for N = 3 from four inflow cases - - the 3x3 and 5x5, the constant coefficient approximation (CCA) with the 5x5 and the no-inflow models. For the CCA case, periodic coefficients (including the extraneous periodicity[16] at $\mu = 0$ in the 5x5 model) are neglected. The 3x3 model data (without CCA) are consistent, in so far as we have the constant coefficient equations at $\mu = 0$ and the damping data approach the no-inflow data for sufficiently large values of $\mu \geq 0.5$ (not shown for $\mu \geq 0.5$). On the other hand, the 5x5 model gives inconsistent set of damping data where the term inconsistency implies three factors. First, the 5x5 model has periodic coefficient equations even at $\mu = 0$. Second, the damping data show increasing effect of inflow with increasing μ. Third, inspite of the low frequency content of the lag regressing mode ($\omega_\zeta \simeq 0.3$), there is appreciable difference between the 5x5 and 3x3 results. It is good to reiterate that, compared to the 3x3 model, the 5x5 model has additional 2/Rev inflow variations which should mildly influence the low-frequency modes. This inconsistency is due to the occurance of spurious periodic terms as a result of discretization of the continuous disc loading by discrete blade loading. Though an exposition of this inconsistency is given elsewhere[16], for completeness, we include briefly the following. For a 5x5 model, the five components of the disc loading harmonics at any instant cannot be uniquely defined by the three blade loadings for N = 3 over one rotor revolution as required by the unsteady conditions of flight dynamics. This inconsistency is due to the growth of such spurious periodic terms and not due to the 4th or 5th, column and row of the 5x5 matrix[16]. This is evident when we compare in figure 2, the 5x5 CCA results with the 3x3 results. The 5x5 CCA removes the inconsistency and the corresponding results exhibit close agreement with the 3x3 data for all μ values.

In figure 3, we continue the preceding discussion for the body roll mode which is also a low-frequency mode. The same inconsistency is also observed here from the roll mode damping data of the 5x5 model. And the 5x5 CCA results show excellent agreement with the 3x3 data. It may be noted that the 5x5 model exhibits the same type of inconsistency with respect to the body pitch mode damping as well[17]. Further, whatever the difference between the two inflow models, they show significant stabilising influence of the dynamic inflow on the lag regressing mode in figure 2 and the destabilising influence on the body roll mode in figure 3. As expected, with increasing advance ratio, the 3x3 model shows decreasing influence of the dynamic inflow in figures 2 and 3.

Before concluding the case for N = 3 with the 5x5 model, we add a comment concerning the lag collective and progressing modes (not shown) though these modes are not conventionally air resonance modes[17]. While the damping of the collective mode remains practically unaffected by the growth of the spurious periodic terms, the high frequency progressing mode ($\omega_\zeta \simeq 1.7$) gets affected much more than the regressing mode since the 5x5

model has 2/Rev variations of inflow[17]. This observation is consistent with the finding of reference 16 as well.

For the three air resonance modes - regressing, roll and pitch - it is convenient to study the two systems with N = 4 and 5 together, as depicted in figures 4, 5 and 6 respectively. Two features are worth mentioning. First, the damping data both from the 3x3 and the 5x5 models exhibit consistency. As a matter of fact, in the hovering ($\mu = 0$), the 5x5 data are identical to the 3x3 data. Also the 3x3 model at $\mu = 0$ reduces to the momentum theory model which has been substantiated by test data. Second, the 3x3 data provide an excellent approximation to the 5x5 model data which exhibit consistency with respect to the three air resonance modes even for N = 4. However, we hasten to add that the 5x5 model for N = 4 (figure 7) does not lead to a consistent rotor wake model though the 3x3 model is consistent. For example, figure 7 refers to the lag collective and lag differential collective modes of the four bladed system with the 3x3 and 5x5 models. Here, extraneous periodic terms from the 5x5 model contaminate only the damping of the lag differential collective mode ($\omega_\zeta = 0.7$), figure 7a. It is good to reiterate that the remaining five modes (N = 4) - - two multiblade lag cyclic modes, the collective lag mode and the two body modes - - have consistent damping data[17]. (Flapping modes are not included here, since flap-damping is not sensitive to the 3x3 and 5x5 dynamic inflow models). Among these consistent damping levels, only that of the lag collective mode is shown in figure 7b, in which the 5x5 and the 5x5 CCA data are practically identical to the 3x3 data. However, for the lag differential collective mode (figure 7a) the 5x5 data are inconsistent. The 5x5 CCA data are consistent though they show increasing deviation from the 3x3 data for large values of μ. This is because, the influence of the legitimate periodic terms of the differential collective mode which remains in the rotating frame increases with increasing μ. One feature of figure 7 merits special mentioning. Though the lag differential collective mode and the lag collective mode have the same reference frequency ($\omega_\zeta = 0.7$), the former mode remains essentially unaffected by dynamic inflow while the latter mode is affected significantly. This is because the differential components remain in the rotating system and does not directly couple with the dynamic inflow which is modelled as a nonrotating feedback[11]. This feature is in sharp contrast to the cases with N = 3 and 5 for which only the lag collective mode remains practically unaffected by spurious terms, figures 2 to 6. We also mention in passing that the 5x5 model for N = 5 (base-line system) gives consistent damping data for all the seven modes[17]. Thus in summary, the 5x5 model though it gives consistent damping data for the air resonance modes for N = 4 as seen from figures 4 to 6, it is a consistent rotor wake model only for $N \geq 5$ as seen from figure 7a.

From figure 8, we once again study the damping of the lag regressing mode for the base-line system with respect to quasi-steady inflow. The 3x3 quasi-steady model provides an excellent approximation to the 5x5 quasi-steady model for all values of μ. And it correlates well with the (unsteady) 5x5 model for $\mu \geq 0.2$, since inflow is virtually quasi-steady for such high μ values.

In the sequel, we select the 3x3 model for three reasons (which apply for all the three air resonance modes). First, the 3x3 model gives consistent damping data for the rotor/body systems with 3, 4 and 5 blades. Second, the 3x3 data correlate extremely well with the 5x5 data of the base-line configuration for the entire flight evenvelope ($0 \leq \mu \leq 0.4$). Third, its quasi-steady model provides good correlation with the corresponding base-line data for $\mu \geq 0.2$ when inflow is known to be quasi-steady.

In phase II we assess how far the number of blades per rotor affects the damping of the air resonance modes. The damping data are shown in figure 9 for N = 3, 4 and 5 in combination with the 3x3 model. It is seen from the figure 9 that air resonance characteristics are virtually independent of the number of blades throughout the flight envelope. Therefore, we will consider only the three bladed rotor/body configurations with the 3x3 model, for the results to follow.

In figure 10 to 13, we discuss the sensitivity of air resonance characteristics to trimming conditions. While figures 10 and 11 refer to the lag regressing and pitch modes of a soft inplane rotor ($\omega_\zeta = 0.7$), figures 12 and 13 refer to the lag regressing and roll modes of a stiff inplane rotor ($\omega_\zeta = 1.4$). Figures 10 to 13, in general, show that the damping levels of all the three air resonance modes are sensitive to trimming conditions, particularly for $\mu > 0.1$. Compared to the damping levels of the body modes, the weakly damped lag mode is the most sensitive. Comparing figure 12 with figure 10, we note that the damping level of the lag regressing mode of the stiff inplane rotor is higher and more sensitive to trimming than that of the soft inplane rotor. While comparing the relative changes in the damping levels between the lag and body modes with respect to trimming conditions, we observe that the lag mode damping level is much less than the body mode damping. For example, for the soft inplane rotor, the damping level of the regressing mode is two orders of magnitude less than the pitch mode damping; compare figure 10 with 11. And, for the stiff inplane rotor, the corresponding lag damping is one order of magnitude less than the roll mode damping; compare figure 12 with 13. Ths phenomenon, viz., higher level of lag damping for a stiff inplane rotor compared to a soft inplane rotor, merits further investigation. As to the body mode, they derive their damping from the flap regressing mode which is well damped. For typical hingeless and bearingless rotors, P varies from 1.1 to 1.2. As a rough approximation for a given advance ratio, the body mode damping levels increase only slightly with increasing P. It is of the order of (P-1).

Figures 10 to 13 depict other significant features as well. In figure 10, under moment trim and untrim conditions, lag mode damping increases with increasing μ, for the soft inplane rotor, a feature consistent with two recent studies[8,9]. However, under propulsive trim condition, the lag mode damping of the same soft inplane rotor shows stabilising trend (compared to the hovering) for $\mu \leq 0.1$ and destabilising trend for $\mu \geq 0.1$. Thus, compared to the hovering condition, the air resonance stability margins for a soft inplane rotor system could be worse for the propulsive trim condition for sufficiently large values of μ (≥ 0.35). As to the damping of the body modes, the pitch mode in figure 11 for $\mu > 0.1$ and the roll mode in figure 13 for all μ values get more and more stabilised with increasing μ for all the three trim conditions. In figure 12, we see that the damping level of the stable lag regressing mode shows increasing stability margins upto $\mu \leq 0.15$ for all the three trim conditions; but for $\mu \geq 0.15$, stability margins decrease rapidly for untrim and moment trim conditions. However, the same stiff inplane rotor under propulsive trim depicts a wavelike behaviour and a simple generalization of such a behaviour is difficult to make. This type of behaviour seems to indicate that the dynamic design of stiff inplane main rotors for air resonance could be a demanding exercise.

To sum up, the damping levels of the lag regressing mode in figure 10 and 12 demonstrate that the air resonance stability margins for high speed flights could be worse when compared to the hovering. This point is

markedly evident for the soft inplane rotor in propulsive trim (figure 10) and for the stiff inplane rotor in moment trim. In other words, these data on damping levels place some doubts on the widely held notion that the hovering flight represents the worst case with respect to air resonance. They show that both soft and stiff inplane rotors merit a detailed air resonance analysis that goes far beyond the analysis of a particular configuration for a specific trim condition.

In phase III, we explore the feasibility of increasing the damping level of the lag regressing mode. Thus, in figures 14 to 16, we respectively treat in moment trim, the effects of structural lag damping, radii of gyration in roll and pitch, Lock number γ ($3\rho acR^2/m$) and mass ratio m_μ. Figure 14 shows an appreciable stabilising influence of lag structural damping. For the same increase in the damping level of the lag regressing mode or stability margin, the amount of structural damping required decreases with the inclusion of dynamic inflow, since dynamic inflow stabilises the lag regressing mode, figure 2. Observe that for a specified stability margin, the amount of structural damping decreases with increasing advance ratio μ. This observation is consistent with the data of figure 2 which shows that under moment trim, stability margin increases with increasing forward speed. Structural lag damping roughly varies as c_d/a and is equivalent to adding a constant term to the actual damping level. Probably, this is the reason why for a given μ, stability margin increases almost linearly with increasing structural damping. Figure 15 refers to the effects of the radii of gyration in roll and pitch ($\bar{r}_s$ and $\bar{r}_c$ respectively) on the stability margin. The damping data are given for the hovering and for the advance ratios of 0.1 and 0.3. As explained earlier, the inclusion of dynamic inflow imparts added stability margin for any given value of $\bar{r}_s$ or $\bar{r}_c$. With increasing body inertia, the so called body 'pendulum' mode[5,8] which is a free-free mode is less influenced by the (P-1) regressing flap mode. In other words, the body acts like a free-free system "where rotor flapping and body rotation react against each other as mass elements" due to the coupling induced by the flap regressing mode. Therefore, in general stability margin increases with increasing values of $\bar{r}_s$ and $\bar{r}_c$. The improvement in stability margin is relatively more sensitive to the increase in $\bar{r}_s$, when compared to the increase in $\bar{r}_c$. This is expected since roll axis is more critical owing to its lower inertia. (For the data in general, the value of $\bar{r}_c$ is twice that of $\bar{r}_s$, see table 3). Figure 16 shows the effects of mass parameters of the blade and the body on the damping level of the lag regressing mode. Figure 16a shows the effects of the mass parameters of the blade for a given blade chord and rotor radius. For a fixed value of P and varying γ, the data in figure 16a although somewhat hypothetical, still give useful information on the effects of the blade mass parameter m on the stability margins. From figure 16a, we see that higher the γ ($3\rho acR^2/m$), the better is the stability margin. With increasing γ, i.e., with decreasing m, the "slenderness" of the rigid blade and consequently the flapping deflection increases, thereby virtually "reducing" the influence of the (P-1) lag regressing mode on the body modes. Figure 16b shows that with increasing mass ratio m_μ, the stability margin decreases. For pure helicopters m_μ is usually close to 0.1. This means, body mass has the dominant value in the ratio between the rotor mass and the total mass (rotor plus body). Thus, increase in the mass ratio causes reduction in the body mass and reduces the body inertia in roll and pitch, thereby increasing the vulnerability of the pendulum mode to air resonance. Therefore, air resonance characteristics worsen with increasing m_μ. Basically, the data of figures 15b and 16b are complementary.

Figures 17 to 23 pertain to phase IV. In these figures, air resonance boundaries without aeroelastic couplings are presented in the 'P - μ'

and '$\mu - \omega_\zeta$' planes and with aeroelastic couplings in the '$P - \omega_\zeta$' plane. Figures 17 and 18 without aeroelastic couplings provide a direct comparison with figures 19 to 23 with such couplings, thus facilitating a better assessment of the effects of couplings on air resonance. Both figures 17 and 18 clearly indicate that air resonance stability boundaries are, in general, improved by dynamic inflow. This is to be expected, since from our earlier discussion (e.g. figure 2) we know that the dynamic inflow stabilises the lag regressing mode which is at best only weakly damped. By comparison, the body modes are better damped, since their damping is derived from the (P-1) flap regressing mode which is well damped. Therefore, this stabilising effect on the lag mode dominates the destabilising effect of dynamic inflow on the body roll or body pitch mode (e.g. figures 3 to 6). Figures 17 and 18 also demonstrate that the extent of stabilization by dynamic inflow for a given advance ratio is more sensitive to P than it is to ω_ζ. This is also to be expected, since dynamic inflow perturbations are sensitive to P and not to ω_ζ. Before we discuss air resonance boundaries in the '$P - \omega_\zeta$' plane with aeroelastic couplings (θ_β, R and θ_ζ) in forward flight, we study the effects of these parameters on the crucial lag regressing mode for different advance ratios. Such data for θ_β, R and θ_ζ are shown in figures 19a, 19b and 19c which depict four important points. First, for a given advance ratio, the stability margins improve with increasing θ_β (compared to $\theta_\beta = -0.4$ in figure 19a). Further, compared to the hovering case and for a given θ_β, this improvement gets better with increasing advance ratio. Second, stability margins decreases very slightly with increasing R for a given advance ratio. In other words, for R = 0 (a rigid blade with all the flexibility in the hub) is only slightly better than for R = 1 (a rigid hub with all the flexibility in the blade) in improving the stability margin for a given μ, at least for P = 1.15 and $\omega_\zeta = 0.7$. This shows that, R is not a very effective parameter in stabilising the lag regressing mode. Third, negative pitch-lag coupling significantly improves the damping level, whereas, positive pitch-flap coupling worsens it. Also, compared to R and θ_β, negative pitch-flap coupling is the most effective parameter in improving the lag damping level. Fourth, computing these coupling parameters without dynamic inflow would lead to highly conservative values, (Figures 17 and 18). While discussing the figures 20 to 23, these points will be referred to as point no.1 of figure 19a etc. Further, all these four points are consistent with three earlier studies[1,4,7] in the hovering without[1,7] and with[4] the inclusion of dynamic inflow. Rather than studying the effects of these parameters on the other two body modes separately, a comprehensive effect of these parameters are presented in the following with respect to air resonance boundaries.

Finally, in figures 20 to 23, we present air resonance boundaries in the '$P - \omega_\zeta$' plane for a typical cruising speed ($\mu = 0.2$). While figures 20 to 22 refer to varying values of θ_β, R and ω_ζ, figure 23 presents a composite view of figures 20 to 22. For hingeless and bearingless rotors, P varies from 1.1 to 1.2 and ω_ζ is close to 0.7. Therefore, we will basically restrict our discussion over a thin rectangular strip in the '$P - \omega_\zeta$' plane with $\omega_\zeta \simeq 0.7$ and $1.1 \leq P \leq 1.2$ (e.g. hatched rectangular strip in figure 23). Figure 20 shows stability boundaries for $\theta_\beta = -0.25$, 0 and +0.25. Comparing the case with $\theta_\beta = 0$ with cases $\theta_\beta = +0.25$ and -0.25, it is seen that the stability margin in the region of interest (i.e. $1.1 \leq P \leq 1.2$, $\omega_\zeta \simeq 0.7$) improves with $\theta_\beta = +0.25$ and basically worsens with $\theta_\beta = -0.25$. This is consistent with point no.1 of figure 19a. From figure 21, we study three cases with R = 0.0, 0.5 and 1. Compared to the case with R = 1, the stability region slightly expands with decreasing values of R (see point no.2 in figure 19b). Generally stated, the value

of R, does not have an appreciable influence on the stability in the region of interest, particularly for $P \geq 1.15$. However, for very low values of P ($1.0 \leq P < 1.04$) and ω_ζ (<0.6), the stability region does improve with decreasing values of R. It appears that for low values of P and ω_ζ, the lower values of R are preferable, while higher values of R ($R \leq 1$), are preferable, for very high values of P (>1.2). In figure 22 we see the effects of θ_ζ. Negative θ_ζ increases the stability region and positive θ_ζ decreases it. (Also see point no.3 of figure 19c). Comparing figure 22 with figures 20 and 21, we note that in improving the air resonance stability boundaries, negative pitch-flap coupling is the most effective parameter and that the hub rigidity parameter R is the least effective one. Finally, we come to figure 23 which is a combination of figures 20, 21 and 22 with R = 0 and 1, $\theta_\beta = +0.25$ and $\theta_\zeta = -0.15$. It is seenthat aeroelastic couplings significantly improve air resonance boundaries (compare with figures 20 to 22 with $\theta_\beta = 0$, R = 0 and 1 and $\theta_\zeta = 0$). As a specific example, the point ($P = 1.15$ and $\omega_\zeta = 0.7$ is basically in the marginally stable region without aeroelastic couplings in figure 20 to 22, and with couplings (figure 23), this point falls well within the stable region. The rotor-hub systems usually represent combinations of soft hubs and flexible blades such that R varies between zero and one. Thus, in summary, it is seen that a judicious combination of negative θ_ζ, and positive θ_β will significantly improve the air resonance characteristics in the required region of interest. Figures 20 to 23 also show that the stability characteristics worsen with high values of P and low values of ω_ζ, as was the case in the hovering[1,4].

In this brief discussion of air resonance boundaries, only one combination (R = 0, $\theta_\beta = 0.25$ and $\theta_\zeta = -0.15$) at $\mu = 0.2$ is selected, which indicates appreciable benefits from aeroelastic couplings. Figure 19 may also give the impression that higher values of these parameters are always preferable to lower values. However, excessive amount of aeroelastic couplings could introduce other types of instabilities. For example, very high values of R together with large negative θ_ζ though beneficial to air resonance at $\mu = 0.2$, is found to produce the instability of the lag-progressing mode in hover for some cases[1]. Here our discussion is restricted to air resonance in forward flight ($\mu = 0.2$) which is a regressing mode type of instability due to body coupling. The challenging problem of finding an almost optimal combination of these coupling parameters that are suitable for all types of aeroelastic instabilities during the entire flight envelope is not the scope of this paper.

4. Concluding Remarks

On the basis of the numerical results presented ($0 \leq \mu \leq 0.4$), the concluding remarks are :

1.a The 3x3 model is a consistent rotor wake model for rotor-body systems with 3, 4 and 5 blades. In other words, all the N multiblade lag modes and the two body modes yield consistent damping data.

1.b The 5x5 model is a consistent model only for rotor/body systems with 5 and more blades. For instance for N = 3, it gives extraneous terms which contaminate the damping level of all the modes except the lag collective mode. For N = 4, these extraneous terms contaminate only the lag differential collective mode.

1.c The 3x3 model provides excellent correlation with the 5x5 model for N = 5 (base-line configuration) with respect to all the modes. Its quasi-steady formulation is also satisfactory for $\mu \geq 0.2$.

2. Air resonance characteristics are independent of the number of blades per rotor.

3. The damping levels of the air resonance modes - - lag regressing, body roll and pitch modes - - are sensitive to trimming conditions. For example, for $\mu \geq 0.1$ the damping levels of the lag regressing mode of a soft inplane rotor in propulsive trim and of a stiff inplane rotor in moment trim show decreasing stability margins. Consequently, the adequacy of the stability margin cannot be ascertained by the air resonance analysis in the hovering alone.

4. Stiff inplane rotors exhibit a variety of air resonance behaviour with respect to trim and a generalised description is difficult to make.

5. Lag structural damping, low blade mass m & high body mass ratio m_μ (consequently high radii of gyration in body roll and pitch) increase stability margins.

6. Dynamic inflow, in general increases the air resonance boundaries. Computation of aeroelastic coupling without the inclusion of dynamic inflow will therefore leads to conservative values.

7. Among the three aeroelastic coupling parameters (θ_β, R, θ_ζ), negative pitch-lag coupling θ_ζ is most effective, and the hub-regidity parameter R, is least effective in improving air resonance stability. For typical hingeless and bearingless rotors ($\omega_\zeta = 0.7$, $1.1 \leq P \leq 1.2$) with the usual combination of soft hub and flexible blades ($0 < R < 1$), the combination with increasing values of negative pitch-lag coupling and positive pitch-flap coupling effectively improve air resonance. The effects of these two coupling parameters ($-\theta_\zeta$ and $+\theta_\beta$) are complementary. Thus, an appropriate combination of these two parameters for all values of R, improves air resonance significantly. (The word 'appropriate' implies that excessive values of these two parameters often affect high frequency lag progressing modes).

5. References

1. Ormiston, R.A., "Aeromechanical Stability of Soft Inplane Hingeless Rotor Helicopters", Third European Rotorcraft and Powered Lift Aircraft Forum, Aix-En-Provence, France, September 7-9, 1977, Paper No. 25.

2. Bousman, W.G., Ormiston, R.A. and Mirick, P.H., "Design Considerations for Bearingless Rotor Hubs", Presented at the 39th Annual Forum of the American Helicopter Society, St.Louis, Missouri, May 13-15, 1983.

3. Bousman, W.G., "An Experimental Investigation of the Effects of Aeroelastic Couplings on Aeromechanical Stability of Hingeless Rotor Helicopters", Journal of the American Helicopter Society, Vol. 26, No. 1, 1981, pp. 46-54.

4. Gaonkar, G.H., Mitra, A.K., Reddy, T.S.R. and Peters, D.A., "Sensitivity of Helicopter Aeromechanical Stability to Dynamic Inflow", VERTICA, The International Journal of Rotorcraft and Powered Lift Aircraft, Vol. 6, No. 1, 1982, pp. 59-75.

5. King, S.P., "Investigations into the Air Resonance Characteristics of a Semi-Rigid Helicopter using a Dynamically Scaled Model", Westland Helicopters Limited, Yeovil, England, DYN/RES/240 N, April 1982.

6. Johnson Wayne, "Development of a Comprehensive Analysis for Rotorcraft-II Aircraft Model, Solution Procedure and Applications", VERTICA, Vol. 5, 1981, pp. 185-216.

7. King, S.P., "The Effect of Pitch-Flap and Pitch-Lag Coupling on Air Resonance", Westland Helicopters Limited, Yeovil, Limited Dynamics Department Report, No. GEN/DYN/RES/005R, July 1971.

8. King, S.P., "Theoretical and Experimental Investigations into Helicopter Air Resonance", 39th Annual Forum of the American Helicopter Society, May 9-11, 1983, Preprint No. A-83-39-21-3000.

9. Lytwyn, R.T., "Aeroelastic Stability Analysis of Hingeless Rotor Helicopters in Forward Flight using Blade and Airframe Modes", Presented at the 36th Annual Forum of the American Helicopter Society, Washington, D.C., May 1980, Preprint No. 80-24.

10. King, S.P., "Aeroelastic Instabilities of Rotor Blades", Final Report on Contract K25A/531/CB 25 A, Westland Helicopters Limited, Yeovil, England, August 1976.

11. Gaonkar, G.H. and Peters, D.A., "Use of Multiblade Coordinates for Helicopter Flap-Lag Stability with Dynamic Inflow", Journal of Aircraft, Vol. 17, No. 2, February 1980, pp. 112-119.

12. Curtiss, H.C. Jr., "Aeroelastic Problems of Rotorcraft", Chapter 7, A Modern Course in Aeroelasticity, by Dowell, E.H., et al, Sijthoff & Noordhoff, The Netherlands, 1978.

13. Gaonkar, G.H., Simha Prasad, D.S. and Sastry, D., "On Computing Floquet Transition Matrices of Rotorcraft", Journal of the American Helicopter Society, Vol. 26, No. 3, July 1981, pp. 29-36.

14. Peters, D.A. and Gaonkar, G.H., "Theoretical Flap-Lag Damping with various Dynamic Inflow Models", Journal of the American Helicopter Society, Vol. 25, No. 3, July 1980, pp. 29-36.

15. Pitt, Dale M., "Rotor Dynamic Inflow Derivatives and Time Constants from Various Inflow Models", USATSARCOM.-TR 81-2, December 1981.

16. Gaonkar, G.H., Sastry, V.V.S.S., Reddy, T.S.R. and Peters, D.A., "On the Adequacy of Modeling Dynamic Inflow for Helicopter Flap-Lag Stability", Eighth European Rotorcraft Forum, Aix-En-Provence, France, August 31 - September 3, 1982, Paper No. 3.11 (To appear in the Journal of the American Helicopter Society, reference is to the Journal version)

17. Nagabhushanam, J., "Rotorcraft Air Resonance in Forward Flight with Various Dynamic Inflow Models and Aeroelastic Couplings" - Ph.D thesis, Indian Institute of Science, Bangalore, India, to be submitted.

18. Nagabhushanam, J., Gaonkar, G.H. and Reddy, T.S.R., "Automatic Generation of Equations for Rotor-Body Systems with Dynamic Inflow for A Priori Ordering Schemes", Seventh European Rotorcraft and Powered Lift Aircraft Forum, Garmisch-Partenkirchen, Federal Republic of Germany, September 8-11, 1981, Paper No. 37.

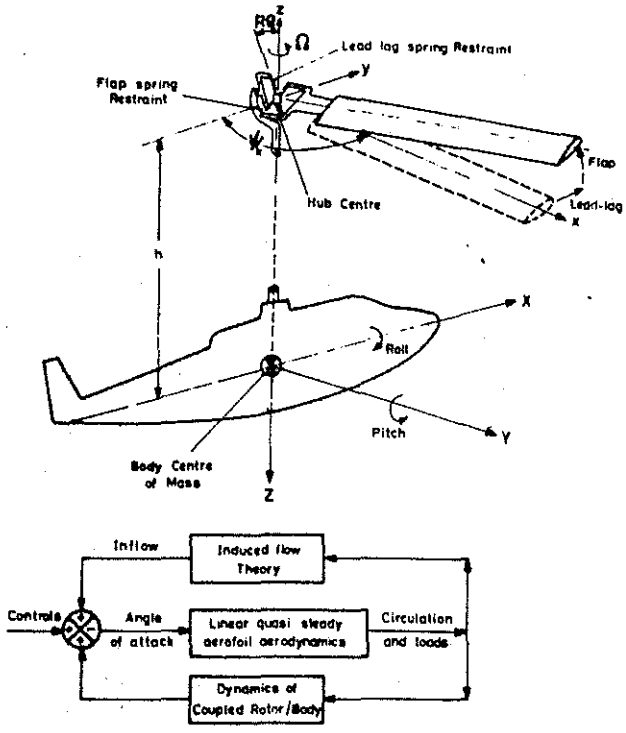

FIG. 1. ROTOR/BODY SCHEMATIC WITH INFLOW BLOCK DIAGRAM.

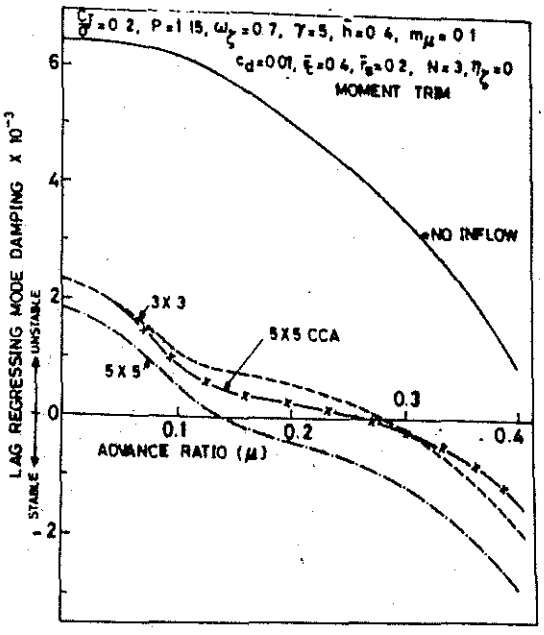

Fig. 2 LAG REGRESSING MODE DAMPING FOR A 3 BLADED ROTOR/BODY SYSTEM WITH THE 3 X 3 AND 5 X 5 INFLOW MODELS.

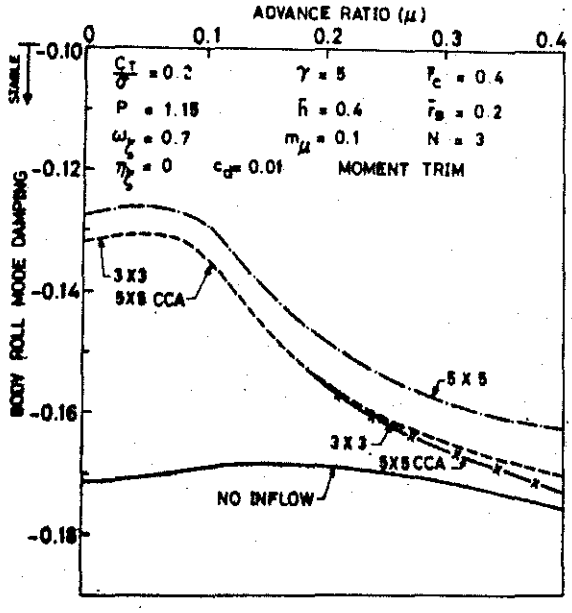

FIG. 3. BODY ROLL MODE DAMPING FOR A 3 BLADED ROTOR/BODY SYSTEM WITH THE 3 X 3 AND 5 X 5 INFLOW MODELS.

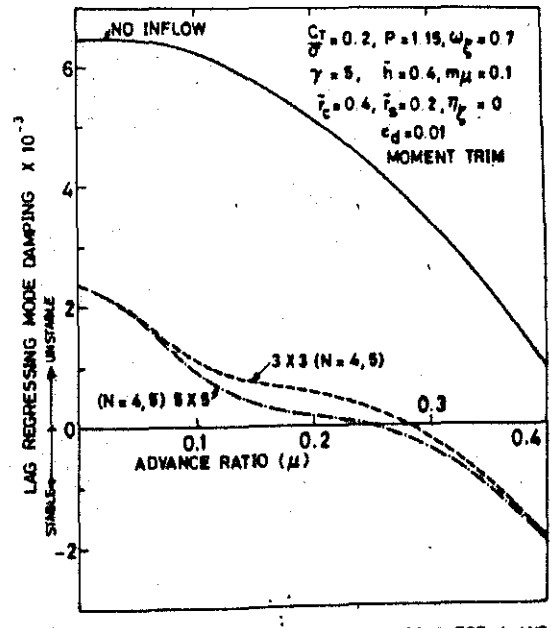

FIG. 4. LAG REGRESSING MODE DAMPING FOR 4 AND 5 BLADED ROTOR/BODY SYSTEMS WITH THE 3 X 3 AND 5 X 5 INFLOW MODELS.

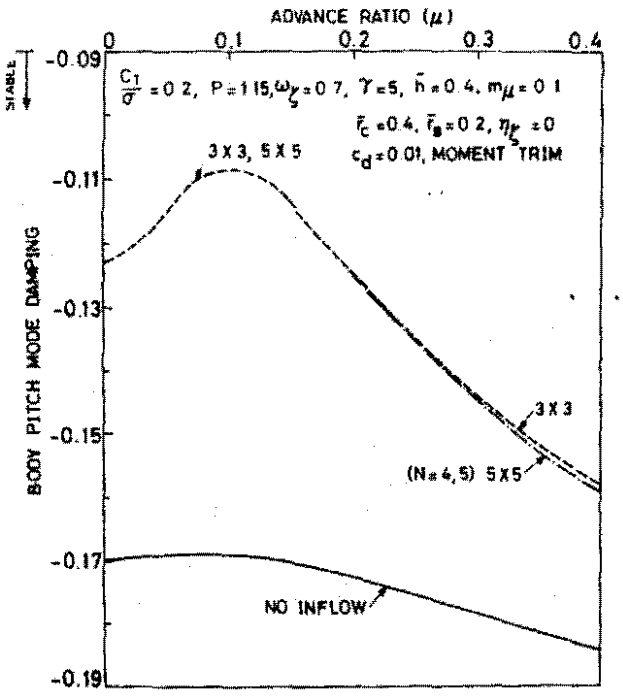

FIG. 5. BODY PITCH MODE DAMPING FOR 4 AND 5 BLADED ROTOR/BODY SYSTEMS WITH THE 3X3 AND 5X5 INFLOW MODELS.

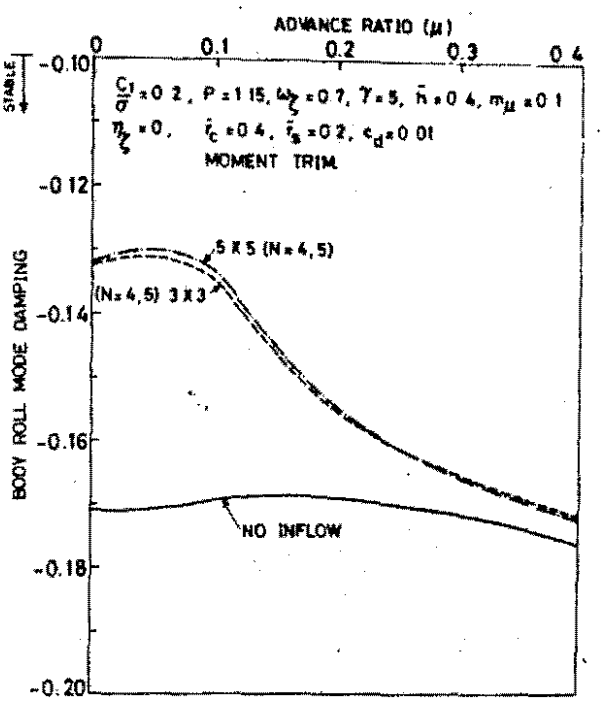

FIG. 6. BODY ROLL MODE DAMPING FOR 4 AND 5 BLADED ROTOR/BODY SYSTEMS WITH THE 3X3 AND 5X5 INFLOW MODELS

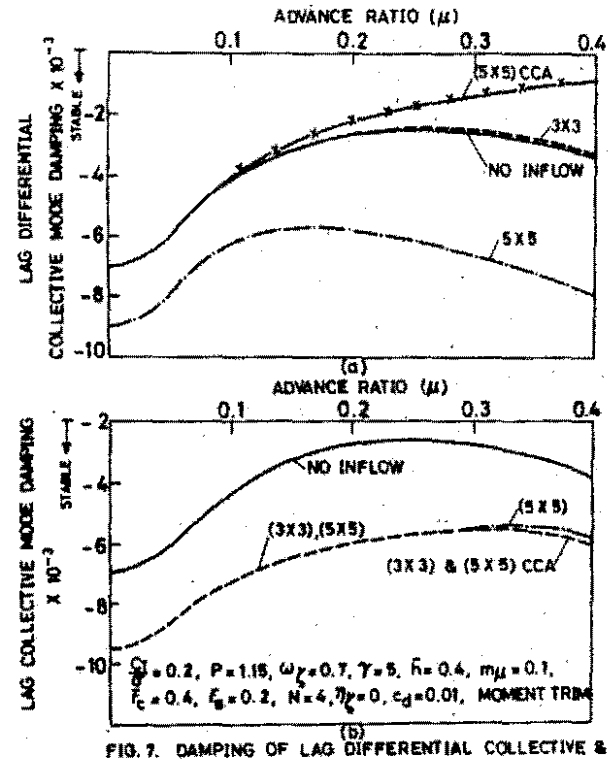

FIG. 7. DAMPING OF LAG DIFFERENTIAL COLLECTIVE & LAG COLLECTIVE MODES OF A 4 BLADED ROTOR/BODY SYSTEM WITH THE 3X3 AND 5X5 INFLOW MODELS.

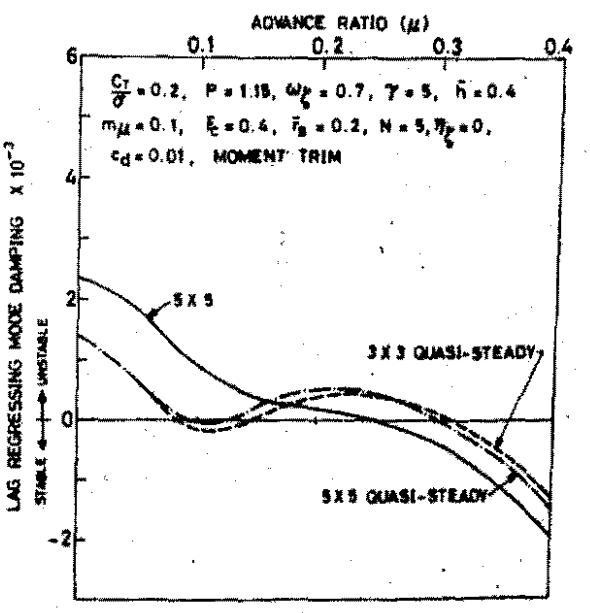

FIG. 8. LAG REGRESSING MODE DAMPING OF A 5 BLADED ROTOR BODY SYSTEM WITH QUASI-STEADY INFLOW MODELS

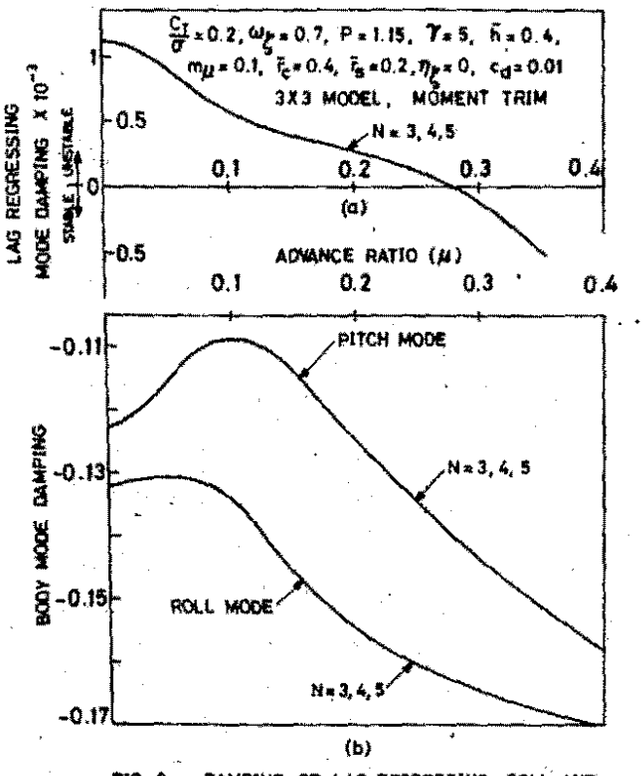

FIG. 9. DAMPING OF LAG REGRESSING, ROLL AND PITCH MODES OF 3, 4 AND 5 BLADED ROTOR/BODY SYSTEMS WITH THE 3X3 INFLOW MODEL.

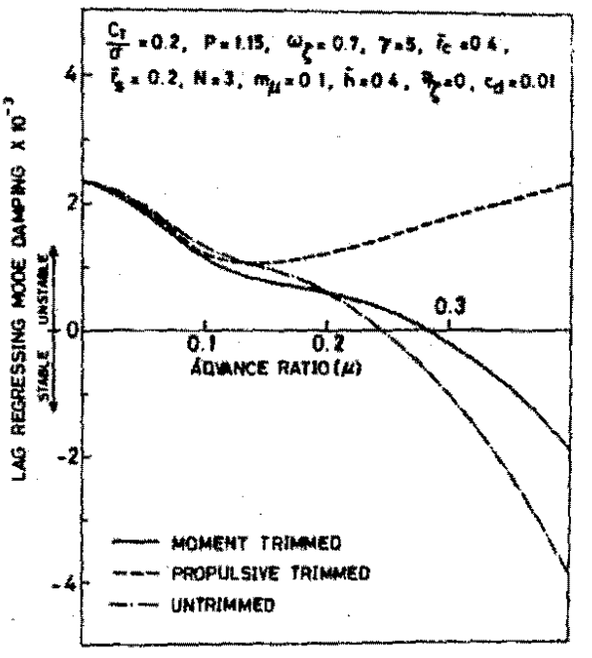

FIG. 10 LAG REGRESSING MODE DAMPING OF A SOFT INPLANE ROTOR/BODY SYSTEM FOR VARIOUS TRIM CONDITIONS.

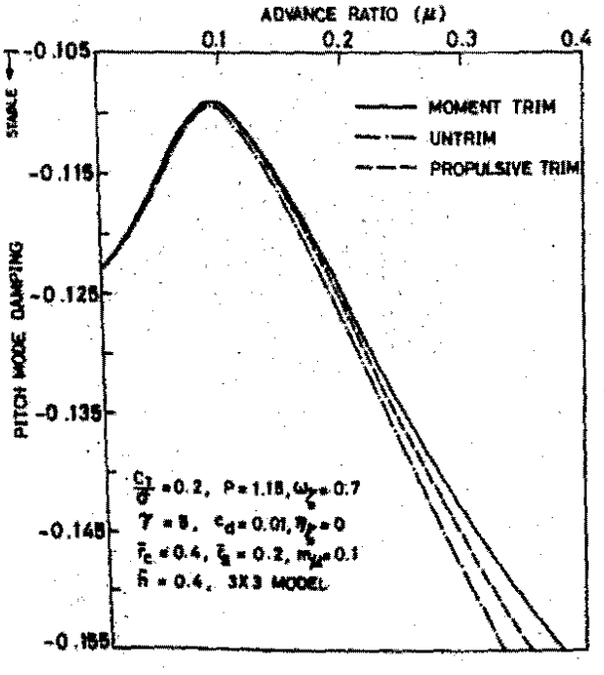

FIG. 11. PITCH MODE DAMPING OF A SOFT INPLANE ROTOR BODY SYSTEM FOR VARIOUS TRIM CONDITIONS.

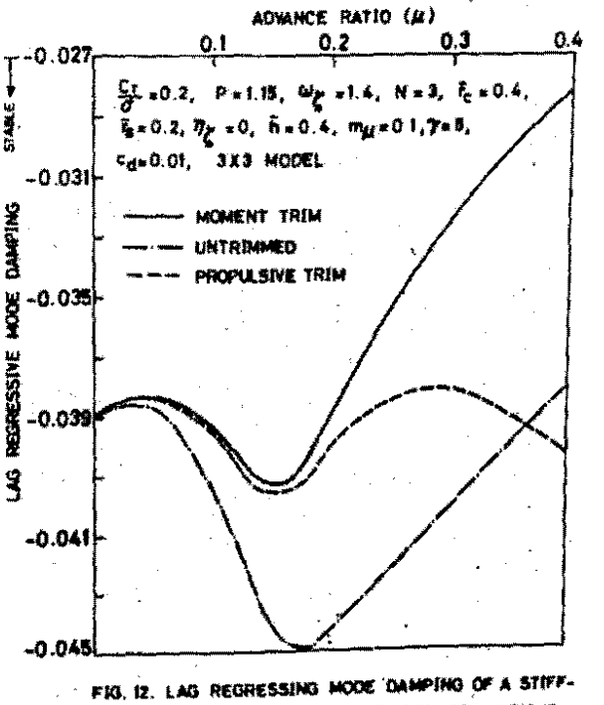

FIG. 12. LAG REGRESSING MODE DAMPING OF A STIFF-INPLANE ROTOR/BODY SYSTEM FOR VARIOUS TRIM CONDITIONS.

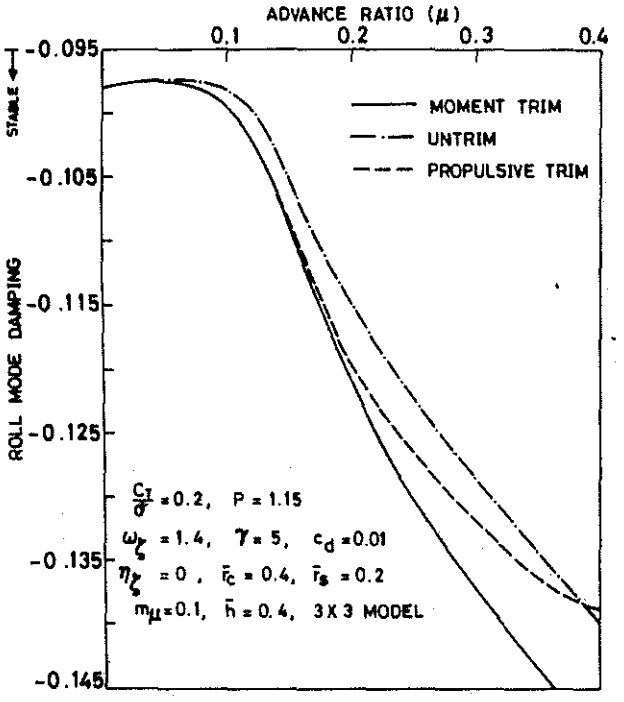

FIG. 13. ROLL MODE DAMPING OF A STIFF INPLANE ROTOR/BODY FOR VARIOUS TRIM CONDITIONS.

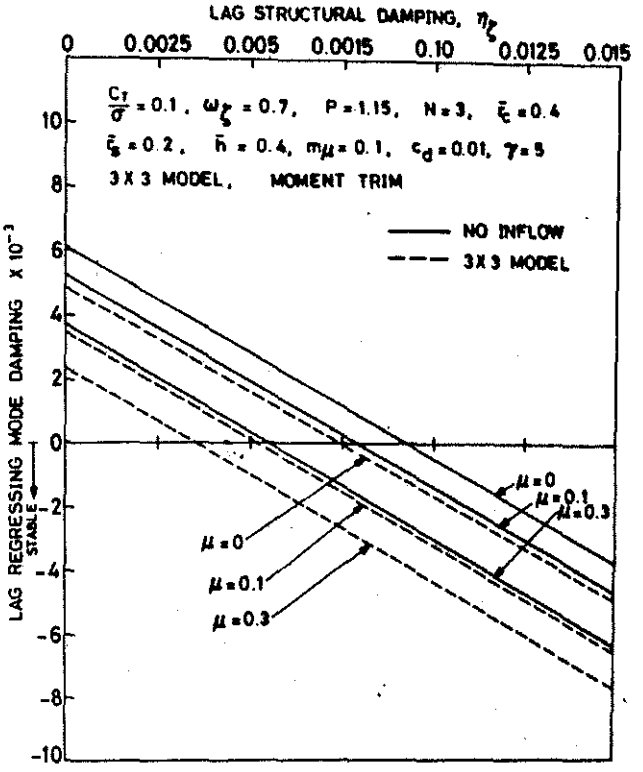

FIG. 14. LAG REGRESSING MODE DAMPING AS A FUNCTION OF THE BLADE LAG STRUCTURAL DAMPING.

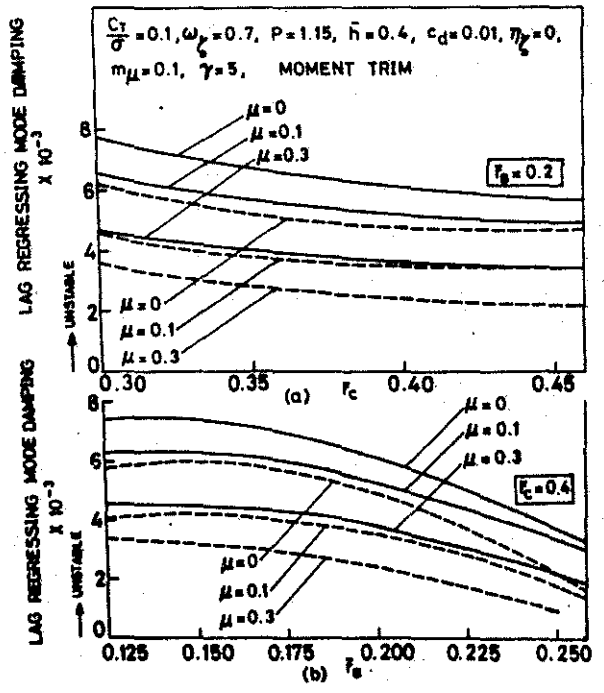

FIG. 15. LAG REGRESSING MODE DAMPING AS A FUNCTION OF THE MASS RADII OF GYRATION IN ROLL AND PITCH.

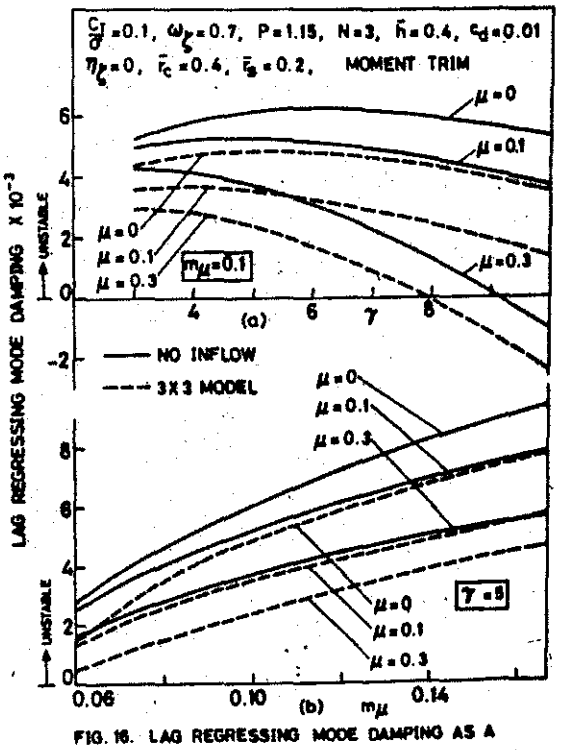

FIG. 16. LAG REGRESSING MODE DAMPING AS A FUNCTION OF LOCK NUMBER γ AND MASS RATIO m_μ.

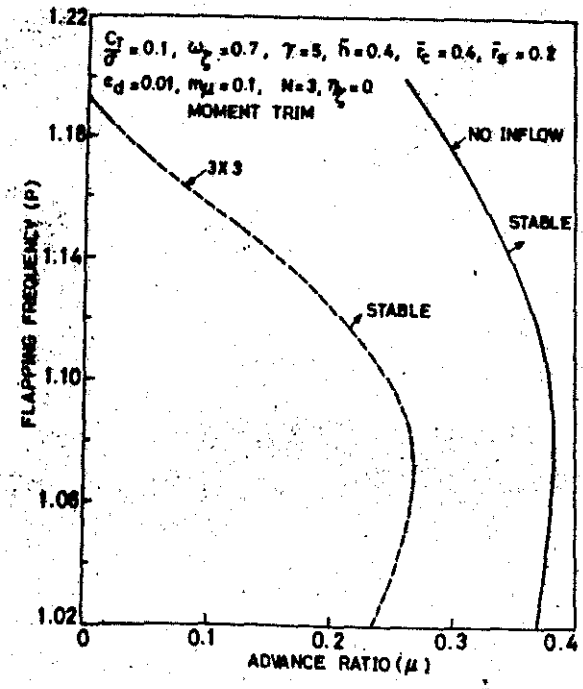

FIG. 17. EFFECT OF FLAPPING FREQUENCY ON AIR RESONANCE BOUNDARIES IN FORWARD FLIGHT WITH AND WITHOUT INFLOW.

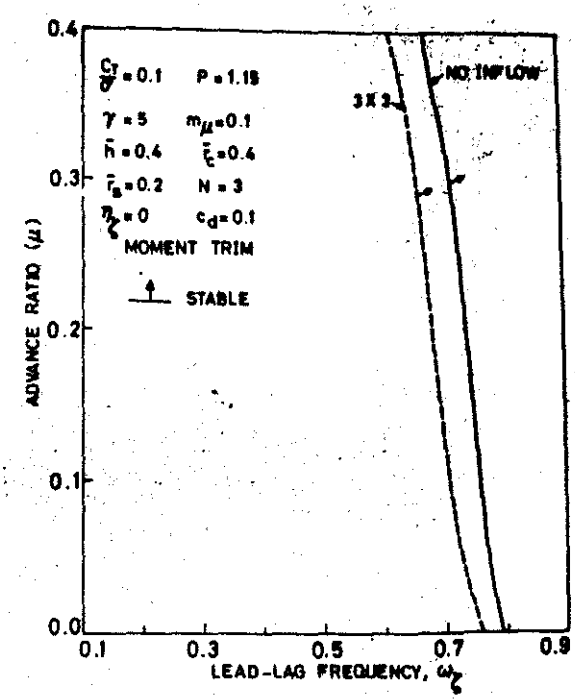

FIG. 18 EFFECTS OF LAG FREQUENCY ON AIR RESONANCE BOUNDARIES IN FORWARD FLIGHT WITH AND WITHOUT INFLOW.

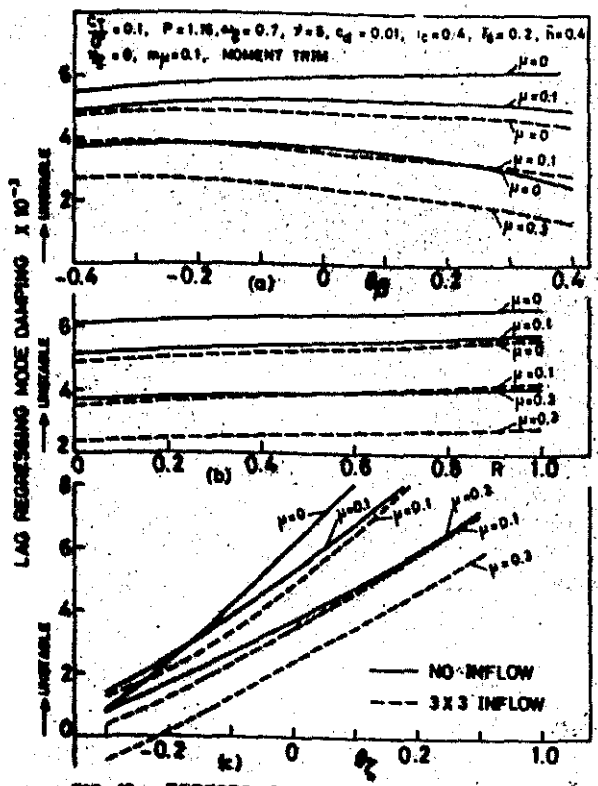

FIG. 19. EFFECTS OF AERO-ELASTIC COUPLINGS ON LAG REGRESSING MODE DAMPING IN FORWARD FLIGHT.

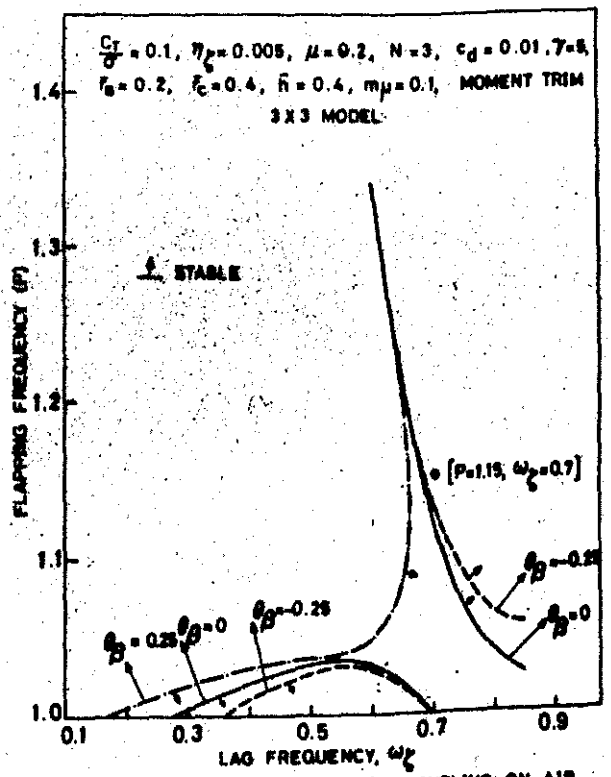

FIG. 20. EFFECTS OF PITCH-FLAP COUPLING ON AIR RESONANCE BOUNDARIES AT μ = 0.2.

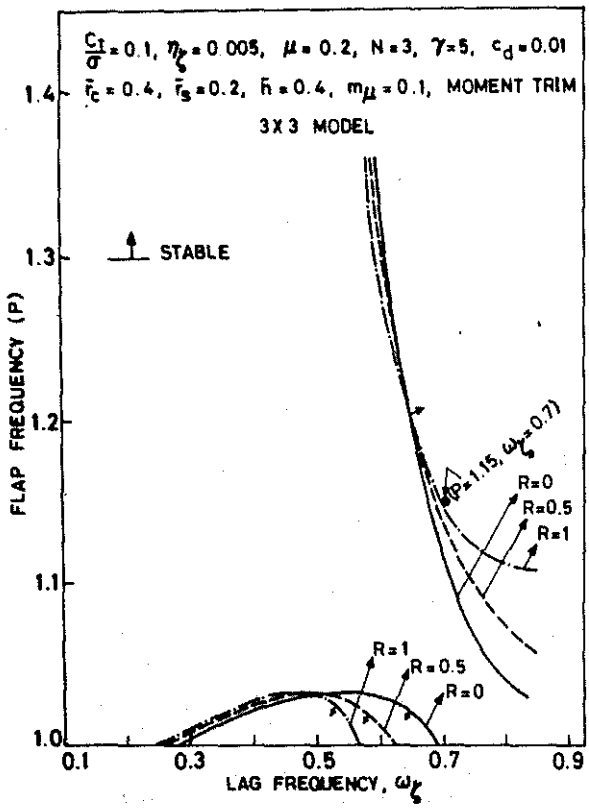

FIG. 21. EFFECTS OF ELASTIC COUPLING PARAMETER R ON AIR RESONANCE BOUNDARIES AT μ = 0.2.

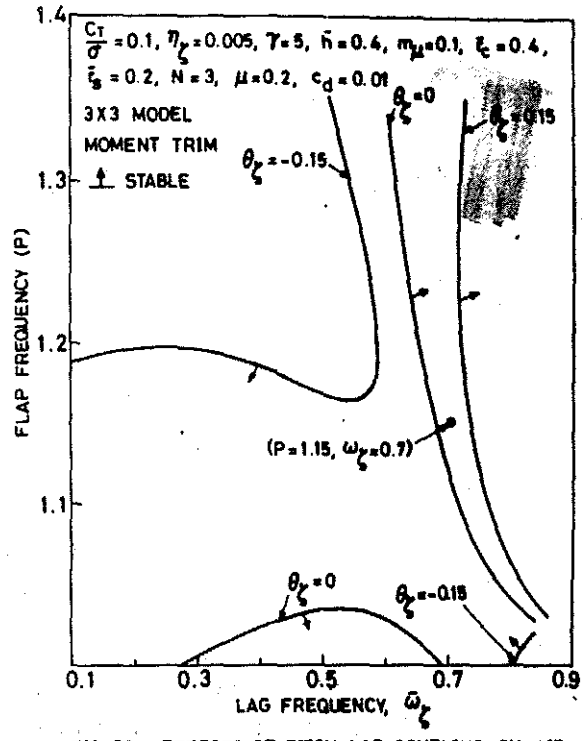

FIG. 22. EFFECTS OF PITCH-LAG COUPLING ON AIR RESONANCE BOUNDARIES AT μ = 0.2.

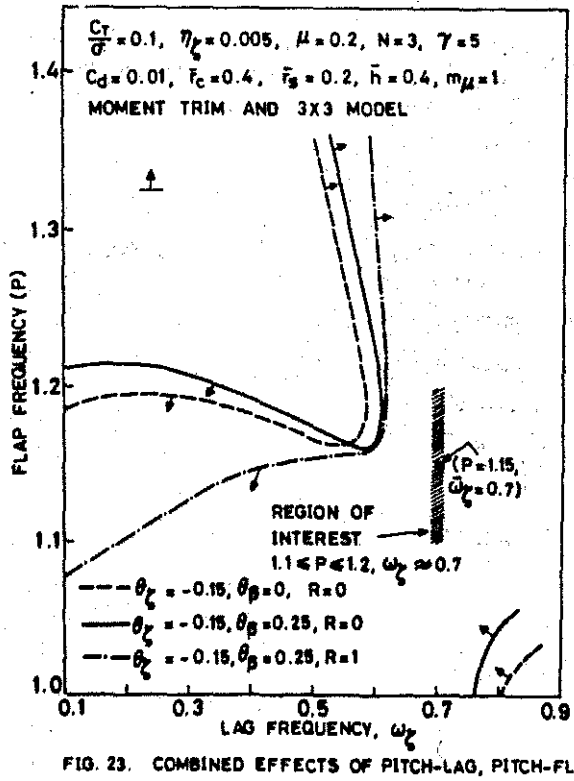

FIG. 23. COMBINED EFFECTS OF PITCH-LAG, PITCH-FLAP AND ELASTIC COUPLINGS ON AIR RESONANCE BOUNDARIES AT μ = 0.2.